Hindawi
Journal of Spectroscopy
Volume 2021, Article ID 8829654, 10 pages
https://doi.org/10.1155/2021/8829654

*Research Article*

# Green Synthesis of Fluorescent Ag Nanoclusters for Detecting $Cu^{2+}$ Ions and Its "Switch-On" Sensing Application for GSH

**Yunpeng Shang**,[1] **Hui Gao**,[1,2] **Lei Li**,[1] **Chaoqun Ma**,[1,2] **Jiao Gu**,[1,2] **Chun Zhu**,[1,2] **Zichen Yang**,[1] **Chengwei Wang**,[1] **Ye Zhang**,[1] **and Guoqing Chen**[1,2]

[1]*School of Science, Jiangnan University, Wuxi, China*
[2]*Jiangsu Provincial Research Center of Light Industrial Optoelectronic Engineering and Technology, Wuxi 214122, China*

Correspondence should be addressed to Guoqing Chen; jncgq@jiangnan.edu.cn

Received 9 September 2020; Revised 21 February 2021; Accepted 2 March 2021; Published 15 March 2021

Academic Editor: Li-June Ming



Herein, we prepared the L-histidine- (His-) protected silver nanoclusters (Ag NCs) by the microwave synthesis method. The synthesis process was rapid, facile, and environmentally friendly. Under 356 nm excitation, the as-prepared Ag NCs exhibited the blue fluorescence, and the fluorescence emission peak was located at 440 nm. The Ag NCs could successfully detect trace copper ($Cu^{2+}$) ions in the aqueous solution and the limit of detection (LOD) was as low as 0.6 pM. Interestingly, the Ag NCs showed a different pH-dependent selectivity for both $Cu^{2+}$ and iron ($Fe^{3+}$) ions with no responses to other heavy metal ions. Furthermore, the as-fabricated fluorescent sensing system was utilized to detect glutathione (GSH, the LOD was 0.8 nM) by using the "switch-on" fluorescence recovery of Ag NCs through adding glutathione (GSH) to the $Cu^{2+}$-Ag NCs solution.

## 1. Introduction

Since heavy metal ions would combine with other toxins in water to produce toxic substances, they could cause serious water pollution leading to a destructive effect on the environment and human health. Among them, iron ($Fe^{3+}$) and copper ($Cu^{2+}$) ions are two of the important heavy metal ions. For children and adults, ingest excessive $Fe^{3+}$ will lead to acute or chronic iron poisoning [1–3]. Excessive $Cu^{2+}$ has toxic effects on brain neurons and causes serious diseases such as Alzheimer's disease, Wilson's disease, and Parkinson's disease [4–6].

Conventional instrumental analysis methods required expensive instrumentation and complicated sample preparations for the trace determination of heavy metal ions [7]. Therefore, finding a fast, sensitive, and selective alternative method is one of the most important research subjects. In recent years, fluorescent nanomaterials have been widely used to develop sensitive fluorescent sensing probes due to their high sensitivity, high selectivity, and wide measurement range [8–13]. Silver nanoclusters (Ag NCs), as novel fluorescent nanomaterials, have been widely used as fluorescent sensing probes in sensing, biorecognition, chemical detection, and catalysis because of their high stability, good water solubility, easy modification, good biocompatibility, and strong bleaching resistance [14–17]. Various preparation methods of Ag NCs including UV-light mediated synthesis and microwave synthesis have been proposed [18–20]. The Ag NCs synthesized with different stabilizing ligands such as DNA, protein, peptide, and amino acid possess different optical properties and application areas [21–26].

For the detection, many methods of detection of $Cu^{2+}$ using the Ag NCs as the probe have been reported. Jing Liu et al. synthesized Ag NCs with PMAA for the detection of $Cu^{2+}$, and the limit of detection (LOD) was 100 nM [27]. Na Xiao et al. synthesized Ag NCs with glutathione for the detection of $Cu^{2+}$, and the LOD was 27 nM [28]. Elaheh Babaee et al. synthesized a dual-emissive ratiometric nanohybrid probe for the detection of $Cu^{2+}$, and the LOD was 7.0 nM [9]. The above-mentioned methods could detect very low concentrations of $Cu^{2+}$, but it is still of great significance to sensitive detection of $Cu^{2+}$.

In this research, we prepared an Ag NCs fluorescent probe for the detection of $Cu^{2+}$ and $Fe^{3+}$ by changing the pH value. The Ag NCs were synthesized using histidine as stabilizer and reductant by microwave synthesis method. Under 356 nm excitation, the Ag NCs solution showed the blue fluorescence with the fluorescent emission peak at 440 nm. The fluorescence intensity response of Ag NCs to the $Cu^{2+}$ and $Fe^{3+}$ was used as the detection signal. A simple pH-tuning method could achieve the selective detection of $Cu^{2+}$ and $Fe^{3+}$. According to this method, the Ag NCs selectively respond to $Cu^{2+}$ and $Fe^{3+}$ at pH = 4.3 and 7, respectively. In addition, as an important tripeptide, glutathione (GSH) has always been a popular detection material [35–37]. Since GSH with thiol bonds could easily form strong complexation with $Cu^{2+}$ [29], we built a fluorescent sensing system to detect GSH. The fluorescence of the Ag NCs was recovered by forming a strong complex of GSH and $Cu^{2+}$. It has application prospects in water pollution and dairy product detection.

## 2. Materials and Methods

*2.1. Chemicals.* Silver nitrate ($AgNO_3$, AR), L-histidine (His, BR), nitric acid ($HNO_3$, AR), hydrochloric acid (HCl, AR), copper chloride ($CuCl_2$, AR), barium chloride ($BaCl_2$, AR), calcium chloride ($CaCl_2$, AR), chromium chloride ($CrCl_3$, AR), iron chloride ($FeCl_3$, AR), potassium chloride (KCl, AR), magnesium chloride ($MgCl_2$, AR), manganese chloride ($MnCl_2$, AR), sodium chloride (NaCl, AR), lead chloride ($PbCl_2$, AR), aluminum chloride ($AlCl_3$, AR), sodium dihydrogen phosphate ($NaH_2PO_4$, AR), and disodium hydrogen phosphate ($Na_2HPO_4$, AR) were purchased from Sinopharm Group Chemical Reagent Co., Ltd. Glutathione reduced (GSH, 99%) and ferrous chloride tetrahydrate ($FeCl_2{\cdot}4H_2O$, AR) were purchased from MACKLIN. Ultrapure water was used throughout all experiments.

*2.2. Synthesis of Ag NCs.* In the experiment, all glassware was thoroughly washed with freshly prepared aqua regia (HCl/$HNO_3$, 3 : 1) and rinsed with ultrapure water prior. In a typical synthesis, an aqueous solution of $AgNO_3$ (0.25 M, 1 mL) was mixed with an aqueous solution of L-histidine (0.125 M, 100 mL) and stirred quickly at room temperature for 10 min. Then the mixture solution was heated (700 W, 2450 MHz) in a microwave oven for 8 min. The color of the solution changed from colorless to light yellow. The solution was then allowed to cool to the ambient temperature before further purification by the dialysis (the dialysis membrane with a molecular mass of 500 Da) for 24 h. The dialyzed solution was freeze-dried to obtain Ag NCs powder and stored in the fridge for further use.

*2.3. Apparatus and Characterization.* Fluorescence emission spectra and excitation spectra were recorded on FLS920 (Edinburgh, Livingston, England). The UV-Vis absorption spectra were measured on the UV-Vis spectrophotometer (Shimadzu, Suzhou, China). The X-ray photoelectron spectra (XPS) were recorded on an ESCALAB 250xi X-ray photoelectron spectrometer (Waltham, MA, USA). Transmission electron microscopy (TEM) image was gained from a JEOL 2100F microscope (Peabody, MA, USA) operating at a maximum acceleration voltage of 200 kV. The domestic microwave oven was from Midea, Guangdong, China.

*2.4. Quantum Yield Measurements.* The quantum yield (QY) of the Ag NCs in water was determined by the reference method. The reference standard material is quinine sulfate (QY = 55% in 0.1 M $H_2SO_4$). And the formula of relative QY is as follows:

$$\phi_x = \frac{A_s}{I_s} \cdot \frac{I_x}{A_x} \cdot \frac{n_x^2}{n_s^2} \cdot \phi_s, \quad (1)$$

where $\phi_x$ is the QY of the Ag NCs and $A$ and $I$ are the absorbance and the integral intensity (excited at 330 nm) of the Ag NCs. $n$ is the refractive index (1.33 in water). The subscript "$s$" represents quinine sulfate, and "$x$" represents the Ag NCs. We prepared a series of different concentrations of the Ag NCs and quinine sulfate solution (adjusting the concentration so that their absorbance was between 0 and 0.2) to make the results more accurate.

*2.5. Detection of $Cu^{2+}$ and $Fe^{3+}$ Ions.* All fluorescence measurement conditions were set as follows: the excitation and emission slit were 4 nm and 6 nm, respectively, the excitation wavelength was 356 nm, and emission was recorded from 380 nm to 600 nm. The typical detection method of $Cu^{2+}$ and $Fe^{3+}$ ions was as follows. The Ag NCs powder was dispersed in water at a concentration of 10 mg/mL for further use. The pH value of the Ag NCs fluorescence probe solution was set at 4.3 for $Cu^{2+}$ and 7.0 for $Fe^{3+}$. Then a certain amount of $Cu^{2+}$ and $Fe^{3+}$ solution was added, and the fluorescence spectrum was recorded 30 minutes later. The ratio of $I_0$ and $I$ ($I_0/I$ or $I/I_0$) was considered to plot the calibration curve and prediction of spiked concentrations, where $I_0$ and $I$ were the fluorescence intensity in the absence and presence of ions. For the selectivity and interference studies, an identical concentration (100 $\mu$M) of the stock solution of other metal ions (i.e., $Na^+$, $Mg^{2+}$, $Ca^{2+}$, $Mn^{2+}$, $Cu^{2+}$, $Cd^{2+}$, $Pb^{2+}$, $Ba^{2+}$, $Fe^{3+}$, $Fe^{2+}$, $Al^{3+}$, and $Cr^{3+}$) was mixed with the probe solution under the same conditions and recorded the fluorescence spectrum 30 minutes later.

*2.6. Detection of GSH.* All fluorescence measurement conditions were set as above. The typical detection method of GSH was as follows. The Ag NCs solution was prepared with a pH = 4.3; then the stock solution of $Cu^{2+}$ (1 mM) was mixed. After 30 minutes, we added a certain amount of GSH solution with different concentrations and recorded the fluorescence spectrum 30 minutes later. The difference between $I$ and $I_0$ ($I - I_0$) was considered; that is, the calibration curve and prediction could be drawn, where $I_0$ and I were the fluorescence intensity of the $Cu^{2+}$-Ag NCs probe system in the absence and presence of GSH.

## 3. Results and Discussion

*3.1. Characterization of Ag NCs.* The fluorescent Ag NCs were prepared by the microwave method with the His as the reductant and stabilizer. The product exhibited a light-yellow solution. In the synthesis process of the Ag NCs, $Ag^+$ was reduced to $Ag^0$ by the imidazolyl groups of the His, and the carboxyl group played an important role in protecting the silver core [8]. All reactants were nontoxic, and the synthesis method was a simple and green process, as shown in Scheme 1. TEM image showed that the Ag NCs were the monodisperse spheres with an average particle size of $4.15 \pm 0.8$ nm (Figure 1). In the HR-TEM image, obvious lattice fringes could be seen with a lattice distance of 2.27 Å (Figure S1).

By XPS, surface composition and elemental analysis for the Ag NCs were characterized. The four peaks of the Ag NCs at 285, 368, 400, and 531 eV (Figure 2(a)) could be attributed to $C_{1s}$, $Ag_{3d}$, $N_{1s}$, and $O_{1s}$, respectively. The results showed that the Ag NCs were mainly composed of C, O, N, and Ag. As shown in Figure 2(b), the two peaks at about 367.8 and 373.9 eV were assigned to the Ag 3d levels. These two peaks could be deconvoluted into four distinct component peaks. The peaks at 368.8 eV ($3d_{5/2}$) and 375.2 eV ($3d_{3/2}$) shown by green line and light blue line were assigned to $Ag^+$. The other peaks at 367.7 eV ($3d_{5/2}$) and 373.8 eV ($3d_{3/2}$) shown by red and dark blue lines were assigned to $Ag^0$. $Ag^0$ and $Ag^+$ could be the core and Ag ions on the surface of the Ag NCs, respectively. Ag ions played an important role in adsorbing the His to stabilize the Ag NCs. The $N_{1s}$ XPS spectrum could be deconvoluted into three distinct component peaks (Figure 2(c)). The peaks at 398 eV, 400 eV, and 408.1 eV shown by red line, green line, and blue line were attributed to C-N, N-H, and -$NO_2$. The peak that appeared at 408.1 eV showed that some of the amino groups of L-histidine reduced $Ag^+$ to $Ag^0$ and the amino groups were oxidized to -$NO_2$ groups [26].

*3.2. The Optical Properties of the Ag NCs.* Optical properties including UV-Vis absorption, fluorescence excitation and emission, and time-resolved fluorescence spectra of the Ag NCs were investigated. As shown in Figure 3(a), the absorption peak at about 300 nm of $AgNO_3$ disappeared, while a new absorption band appeared at 250–300 nm. In addition, the absorption peak near 411 nm was the characteristic surface Plasmon resonance (SPR) peak of large-size silver nanoparticles [30, 31]. There was no absorption peak emerging around 411 nm, as Figure 3(a) shows. Therefore, it could prove that the product was the Ag NCs with a core diameter of less than 2 nm. The fluorescence spectra of the Ag NCs solution, the His solution, and the solution mixed with His and $AgNO_3$ were compared under the excitation at 365 nm. The fluorescence of the His solution and the solution mixed with His and $AgNO_3$ could not be observed under the same excitation (Figure S2). Therefore, the Ag NCs were the fluorescence substance in the solution. As shown in Figure 3(b), the fluorescence emission reached the maximum at 356 nm excitation with the emission maximum at 440 nm. In addition, the Ag NCs solution under natural light had no obvious luminescence, while under ultraviolet (365 nm), it exhibited the blue fluorescence. Using quinine sulfate in 0.1 M $H_2SO_4$ as a reference, the QY was 5.2%. Time-resolved fluorescence spectrum (Figure 3(c)) showed that the fluorescence lifetime of the Ag NCs was 1.13 ns (13.87%), 3.98 ns (51.57%), and 8.25 ns (34.56%), and the average lifetime was 5.06 ns (Table S1).

*3.3. Effects of Solution pH on Detection of $Cu^{2+}$ and $Fe^{3+}$ by the Ag NCs.* The influence of the solution pH was examined to optimize the sensing conditions. It was found that the sensitivity and selectivity of the Ag NCs detection of $Cu^{2+}$ and $Fe^{3+}$ were dependent on the pH value. The Ag NCs had a high response to $Cu^{2+}$ at pH = 4.3 (Figure 4(a)) and to $Fe^{3+}$ at pH = 7 (Figure 4(b)). And at those two pH value conditions, the effect of other metal ions on the fluorescence intensity of the Ag NCs was very small. Therefore, pH = 4.3 and pH = 7 were selected as the detection condition for $Cu^{2+}$ and $Fe^{3+}$ ions, respectively. The results showed that the selectivity to $Cu^{2+}$ and $Fe^{3+}$ could be achieved by controlling the pH value of the Ag NCs fluorescent probe solution without adding other chelating agents.

After adding $Cu^{2+}$ and $Fe^{3+}$ ions, the Ag NCs solution exhibited different responses under different pH value. It could be attributed to the different binding mechanism between the two ions and His. According to the previous reports, His presented a strong binding affinity with $Cu^{2+}$ via coordinating $Cu^{2+}$ through the amino group and the imidazole ring [32]. The terminal amino and the imidazole nitrogen donors could form a six-membered chelate. In the presence of excess ligand, bis(ligand) complex could be formed in slightly acidic samples. When the pH increased, the amino group and the imidazole ring were deprotonated [33]. It could decrease the $Cu^{2+}$-binding affinity with His. In addition, the $Fe^{3+}$ could coordinate with carboxyl groups of the surface ligand. In acidic media, the carboxyl groups were easily protonated at a low pH value. Hence, neutral media were the most suitable condition for Ag NCs detecting $Fe^{3+}$ [8, 34]. In alkaline media, $OH^-$ and $Fe^{3+}$ ($Cu^{2+}$) could form precipitation. It could result in complexing capability getting weak. Hence, when pH = 4.3 and 7, the Ag NCs showed a high response to $Cu^{2+}$ and $Fe^{3+}$, respectively.

*3.4. Calibration Curves and Detection Limits for Sensing $Cu^{2+}$ and $Fe^{3+}$.* The above-mentioned optimal pH conditions for the $Cu^{2+}$ and $Fe^{3+}$ were then employed to construct their calibration curves based on the as-prepared Ag NCs. When the concentration of $Cu^{2+}$ was less than $1 \times 10^{-6}$ M (Figure 5(a)), the fluorescence intensity gradually increased with the increasing concentration of the $Cu^{2+}$. When the concentration of $Cu^{2+}$ was more than $1 \times 10^{-3}$ M, the fluorescence intensity decreased with the increasing of the concentration of $Cu^{2+}$ (Figure S3). Figure 5 showed that the fluorescence emission intensity ratio was sensitively and proportionately increased with an increasing concentration of $Cu^{2+}$ at 440 nm. A linear relationship from $1 \times 10^{-12}$~$1 \times 10^{-6}$ M could be described ($I/I_0$) = 0.0155 [log $C$] + 1.294 ($R^2$ = 0.9897). And the LOD for $Cu^{2+}$ was as low as 0.6 pM.

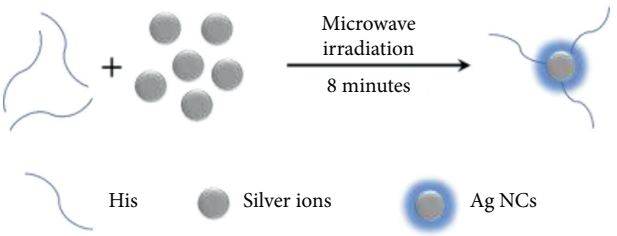


Scheme 1: Schematics of the formation of the Ag NCs.

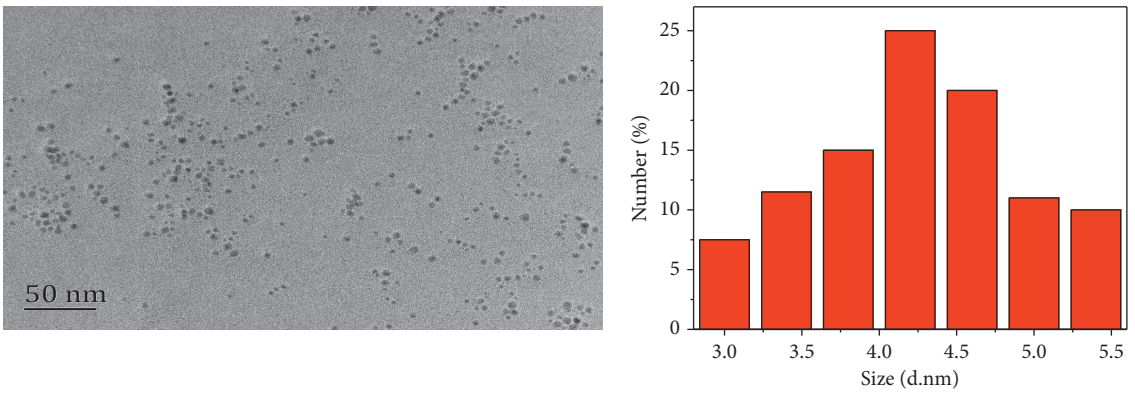


Figure 1: (a) TEM images of the Ag NCs. (b) The particle size distribution histogram of the Ag NCs.

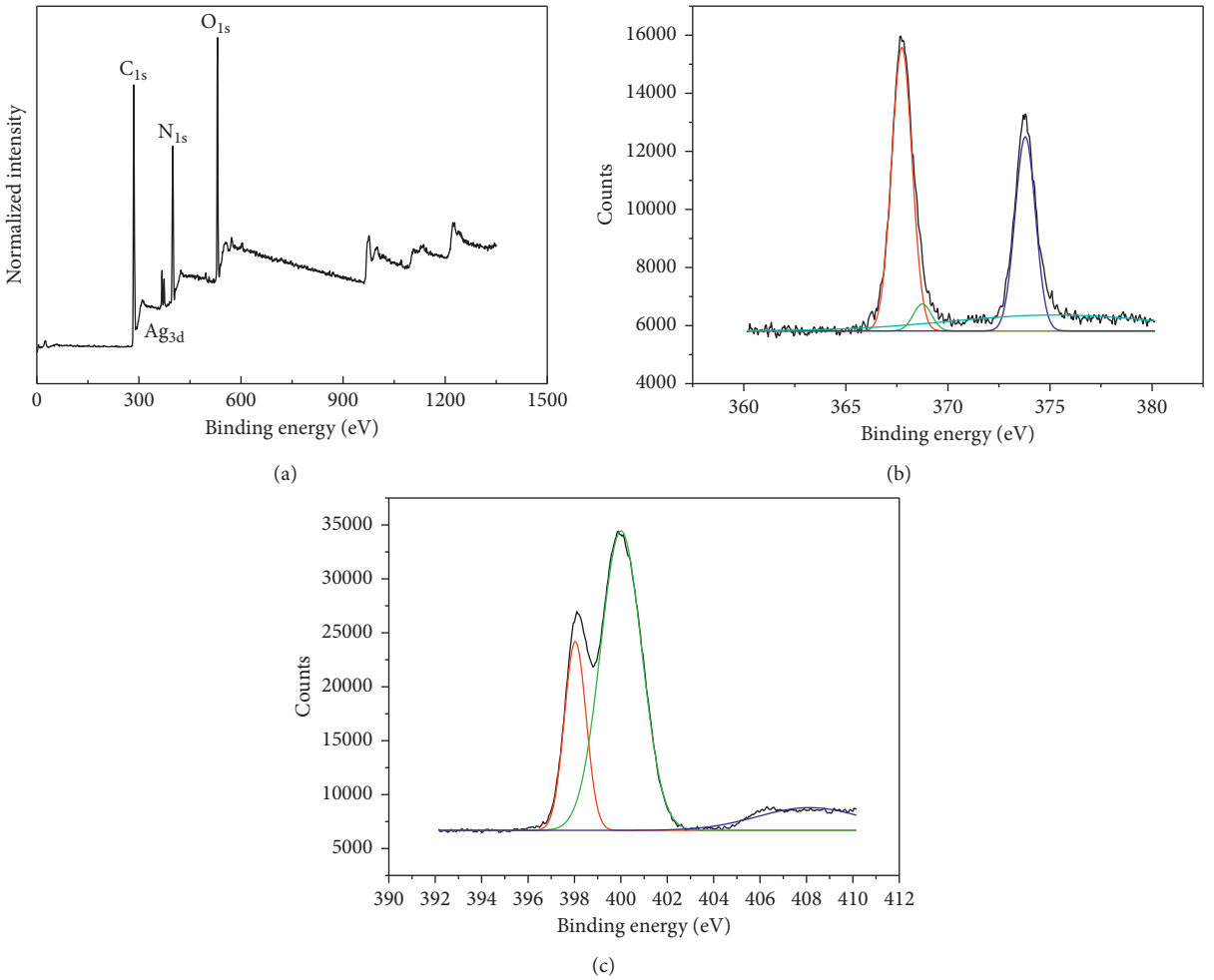


Figure 2: (a) XPS survey spectrum of the Ag NCs. (b-c) High-resolution XPS spectra of $Ag_{3d}$ and $N_{1s}$, respectively.

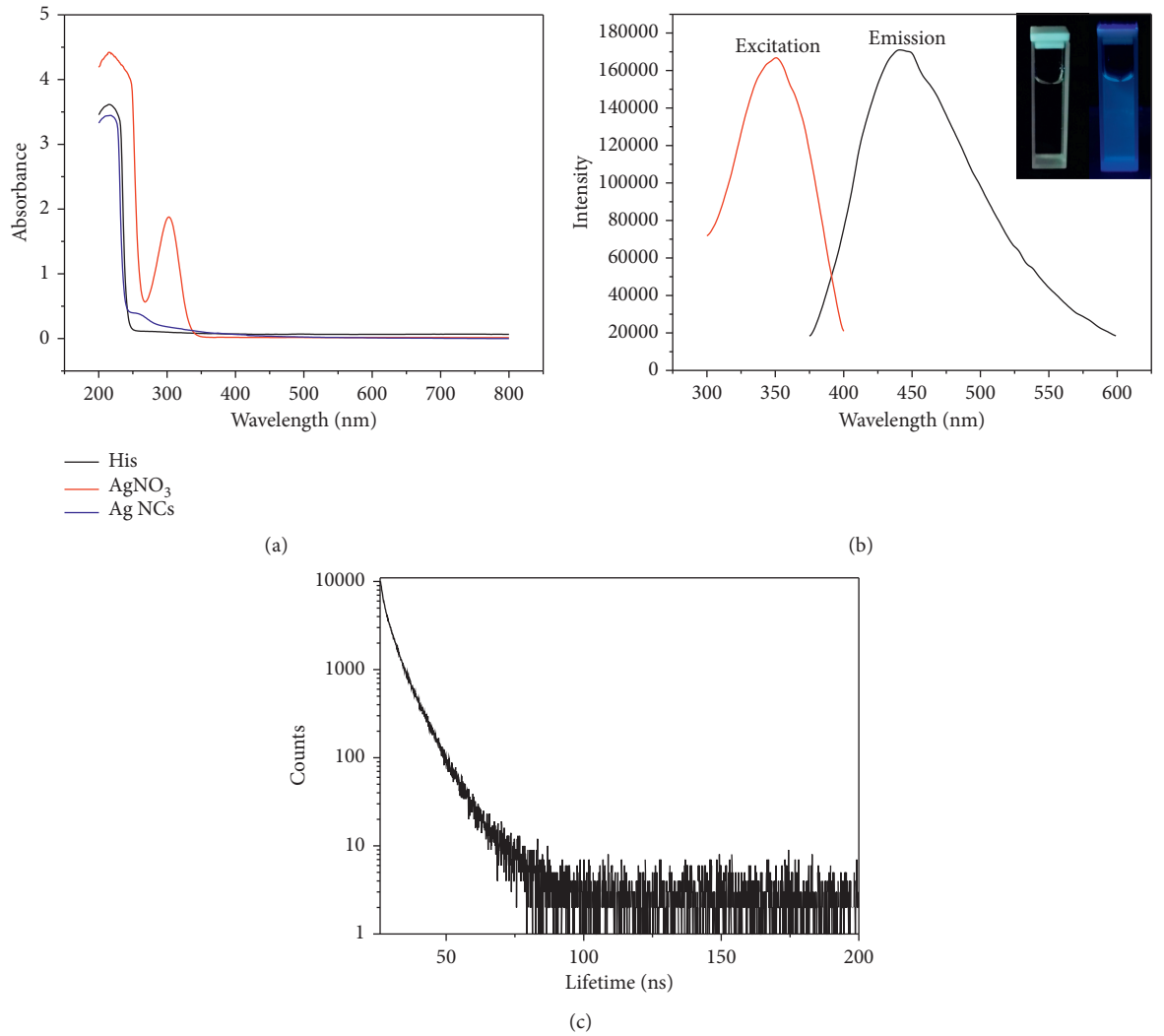


Figure 3: (a) UV-Vis absorption spectrum of His (black), $AgNO_3$ (red), and the Ag NCs (blue) solution. (b) The PL excitation and emission spectra of the Ag NCs. The inset in (b) is the Ag NCs solution under natural light (left) and under ultraviolet (right). (c) Time-resolved fluorescence spectrum of the Ag NCs.

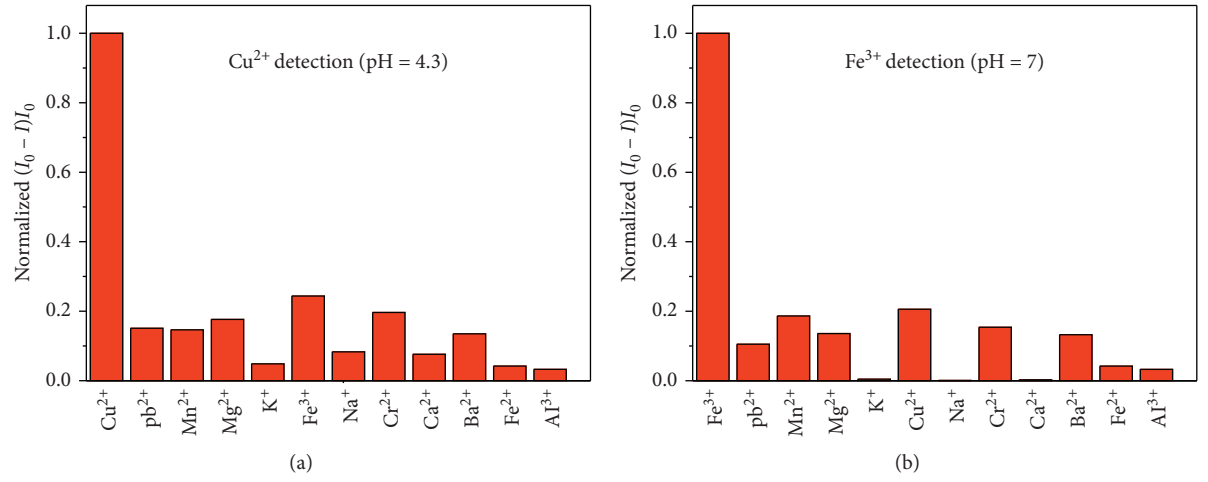


Figure 4: Selectivity patterns of the Ag NCs to $Cu^{2+}$ at pH = 4.3 (a) and $Fe^{3+}$ at pH = 7 (b). All metal ions concentrations were 100 $\mu$M.

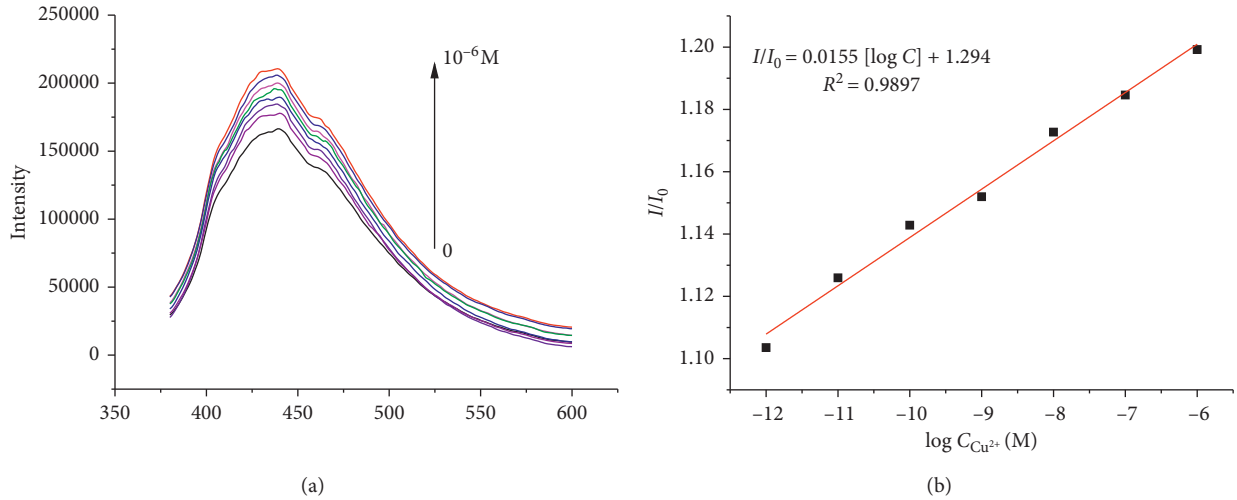


FIGURE 5: (a) Fluorescence response of the Ag NCs upon addition of different concentrations of $Cu^{2+}$ from bottom to top: $0.1 \times 10^{-12}$ M, $1 \times 10^{-11}$ M, $1 \times 10^{-10}$ M, $1 \times 10^{-9}$ M, $1 \times 10^{-8}$ M, $1 \times 10^{-7}$ M, and $1 \times 10^{-6}$ M. (b) The linear calibration ranges of the fluorescence intensity ratio to $Cu^{2+}$ concentrations.

When the pH = 7 (Figure 6(a)), the fluorescence intensity decreased with the increasing concentration of $Fe^{3+}$ ions. The fluorescence intensity ratio of the Ag NCs at pH = 7 (Figure 6(b)) possessed a linear relationship with the concentration of $Fe^{3+}$ from 100~1000 $\mu$M with a regression equation of $(I_0/I) = 0.0008\ [C_{Fe}{}^{3+}] + 0.9353$ ($R^2 = 0.9944$). The LOD for $Fe^{3+}$ is 9.8 $\mu$M.

The Ag NCs showed different response mechanism for the above two $Cu^{2+}$ concentration ranges. The fluorescence of Ag NCs was enhanced at low concentration (under 1 $\mu$M) of $Cu^{2+}$ and quenched at high concentration (over 1 mM) of $Cu^{2+}$. The different response of the Ag NCs toward the two kind $Cu^{2+}$ concentration ranges could be attributed to the different binding degree of $Cu^{2+}$ with His. As shown in Figure S4, after adding two concentrations of $Cu^{2+}$ (1 mM and 1 nM), the lifetimes of the Ag NCs samples changed. It proved that the fluorescence dynamic quenching of the Ag NCs due to the Cu2+ was binding to His. The proposed mechanisms for the interaction of the Ag NCs by two concentrations of $Cu^{2+}$ were further confirmed by the analysis of UV-Vis absorption spectrum and TEM images. As shown in Figure 7, when the concentration of $Cu^{2+}$ was 1 mM, the aggregation of the Ag NCs was indicated because the absorbance of the absorption peak at 250–300 nm was enhanced. The aggregation of the Ag NCs in the presence of $Cu^{2+}$ (Figure S5(a)) could be attributed to the interaction between the His shell of the Ag NCs and $Cu^{2+}$. The quenched fluorescence could be attributed to aggregation of the Ag NCs by the simple coordination of $Cu^{2+}$ with the amino groups of the His ligand. When the concentration of $Cu^{2+}$ was 1 nM, it was indicated that the Ag NCs were without aggregation because the absorption spectra at 250–300 nm were unchanged (Figure 7). It could be seen that the Ag NCs still have good dispersion in the presence of $Cu^{2+}$ (Figure S5(b)). This might be due to the fact that the low concentration of $Cu^{2+}$ was not enough to induce the Ag NCs aggregation. In addition, the absorption peak of the π bond groups at 200 nm decreased (Figure 7). It could be attributed to the addition of $Cu^{2+}$ which only improved the spatial structure of the functional groups on the surface of the Ag NCs. It was supposed that the fluorescence intensity was enhanced due to the spatial structural change of the Ag NCs.

*3.5. Application to Water Samples.* As mentioned above, the fluorescence of Ag NCs was enhanced in the presence of the $Cu^{2+}$ at a low concentration without interference from other ions. Therefore, the proposed probe could be used for the detection of $Cu^{2+}$ in real samples. To verify this, mineral water samples spiked with different concentrations of $Cu^{2+}$ were examined. Table 1 summarizes the obtained results for the prediction of the concentrations of $Cu^{2+}$. As shown in Table 1, there was an excellent percent recovery for $Cu^{2+}$ in the mineral water samples. Therefore, the probe displayed high capability for the determination of the copper ions in real samples.

*3.6. Comparison of the Ag NCs with Previously Reported Fluorescent Nanoprobes.* The merits such as linear range, detection limit, and selectivity of the proposed Ag NCs for $Cu^{2+}$ and $Fe^{3+}$ are summarized in Table 2. Compared with other fluorescent probes reported for the determination of two ions, according to Table 2, the reported probes' selective determination of two ions in the aqueous solution was to mask one of these ions with a masking agent such as EDTA. In most cases, EDTA as an efficient $Cu^{2+}$ and $Fe^{3+}$ chelating agent could not be used to selectively determine $Cu^{2+}$ and $Fe^{3+}$.

This work proposed a method for selective determination of $Cu^{2+}$ and $Fe^{3+}$ only by controlling the solution pH value. For example, in the acidic media, the easier protonation of carboxyl groups at low pH value resulted in the inability of $Fe^{3+}$ to coordinate with carboxyl groups. Therefore, $Fe^{3+}$ could not disturb the determination of $Cu^{2+}$ ions.

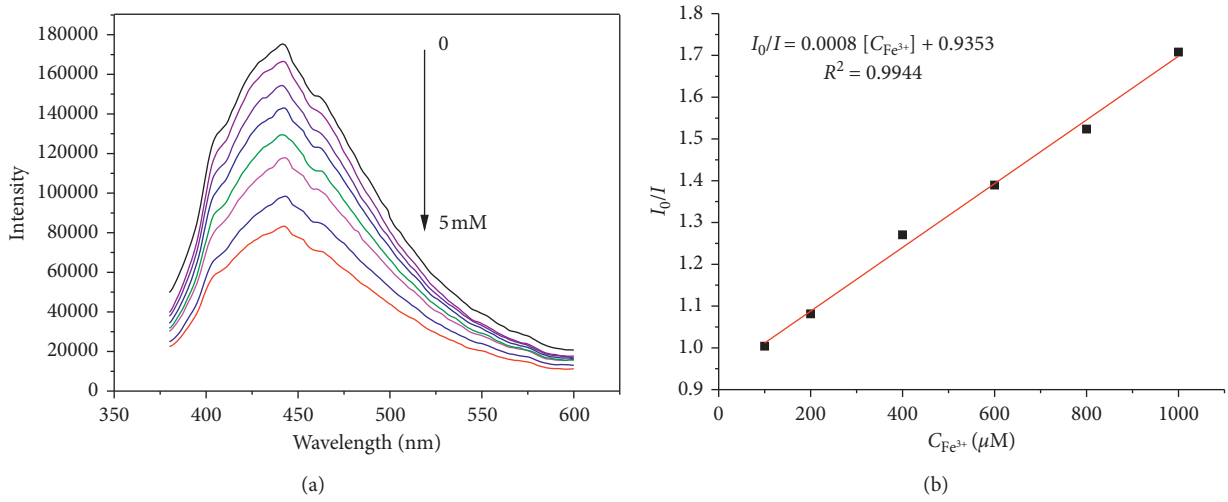


Figure 6: (a) Fluorescence response of the Ag NCs upon addition of different concentrations of $Fe^{3+}$ from top to bottom: 0 mM, 0.1 mM, 0.2 mM, 0.4 mM, 0.6 mM, 0.8 mM, 1 mM, and 5 mM. (b) The linear calibration ranges of the fluorescence intensity ratio to $Fe^{3+}$ concentrations.

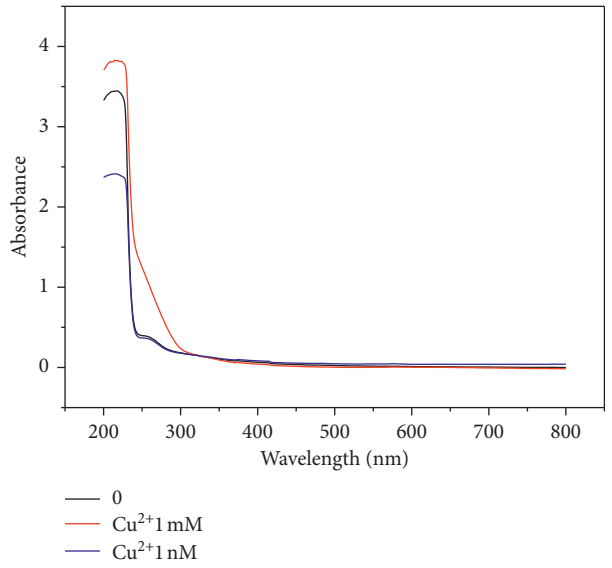


Figure 7: UV-Vis absorption spectrum of the Ag NCs upon addition of different concentrations of $Cu^{2+}$.

Table 1: Application of the probe for $Cu^{2+}$ in real samples (data are average of three replicate measurements).

| Sample | $Cu^{2+}$ (pM) | | Recovery (%) |
|---|---|---|---|
| | Added | Found | |
| Mineral water | 1 | 1.07 (±0.1) | 107 |
| | 100 | 103 (±11) | 103 |
| | 10000 | 10073 (±110) | 101 |

*3.7. Calibration Curves and Detection Limits for Sensing of GSH.* Since GSH is a very important antioxidant, $Cu^{2+}$-Ag NCs sensing system was further utilized for the detection of GSH. A "switch-on" effect on recovery of the fluorescence of Ag NCs could be expressed in this sensing system. A wide detection range and low detection limit could be obtained by this method. As shown in Figure 8, the fluorescence intensity of the Ag NCs was obviously recovered at 440 nm. A linear relationship for GSH was obtained from 1 nM to 8 mM with a regression equation of $(I - I_0) = 12107.6–1234.49(–\log 10\ (C))$ ($R^2 = 0.9888$), where $I_0$ and $I$ were the fluorescence intensity of the $Cu^{2+}$-Ag NCs probe system in the absence and presence of GSH. The LOD for GSH was 0.8 nM.

Table 2: Comparison of Ag NCs probe for the detection of $Cu^{2+}$ and $Fe^{3+}$ with previously reported fluorescent-based probes in aqueous solution.

| Probe | Detected ion | Linear range | LOD (nM) | Selectivity | Ref |
|---|---|---|---|---|---|
| Ag NCs | $Cu^{2+}$ | — | 10 | With no selectivity over ions even with the help of EDTA | [38] |
| | $Hg^{2+}$ | 0~100 nM | 5 | | |
| Au-Ag NCs | $Cu^{2+}$ | 0.5 nM~2.5 $\mu$M | 0.3 | Selective determination of $Hg^{2+}$ by masking $Cu^{2+}$ with EDTA | [39] |
| | $Hg^{2+}$ | 0.2 nM~2.5 $\mu$M | 0.1 | | |
| Ag NCs | $Cu^{2+}$ | 0.1 nM~20 $\mu$M | 28 | Masking $Hg^{2+}$ with thymine and masking $Cu^{2+}$ with potassium pyrophosphate | [40] |
| | $Hg^{2+}$ | 0.1 nM~10 $\mu$M | 35 | | |
| Ag NCs | $Cu^{2+}$ | 0~1 $\mu$M | 2.8 | Masking $Cu^{2+}$ with EDTA for selective determination of $Hg^{2+}$ | [41] |
| | $Hg^{2+}$ | 0.01~0.5 $\mu$M | 1.0 | | |
| Ag NCs | $Fe^{3+}$ | 0.5 $\mu$M~20 $\mu$M | 0.12 | — | [42] |
| Au NCs and | $Fe^{3+}$ | 5 $\mu$M~1 mM | 1.11 | Masking $Fe^{3+}$ with EDTA for selective determination of $Hg^{2+}$ | [34] |
| Au/Ag NCs | $Hg^{2+}$ | 5 nM~5 $\mu$M | 1.56 | | |
| Ag NCs | $Cu^{2+}$ | 1 pM~1 mM | 0.6 | Switching the selectivity by controlling solution pH (pH = 4.3 for $Cu^{2+}$ determination and pH = 7 for $Fe^{3+}$ determination) | This work |
| | $Fe^{3+}$ | 100~1000 $\mu$M | 9.8 | | |

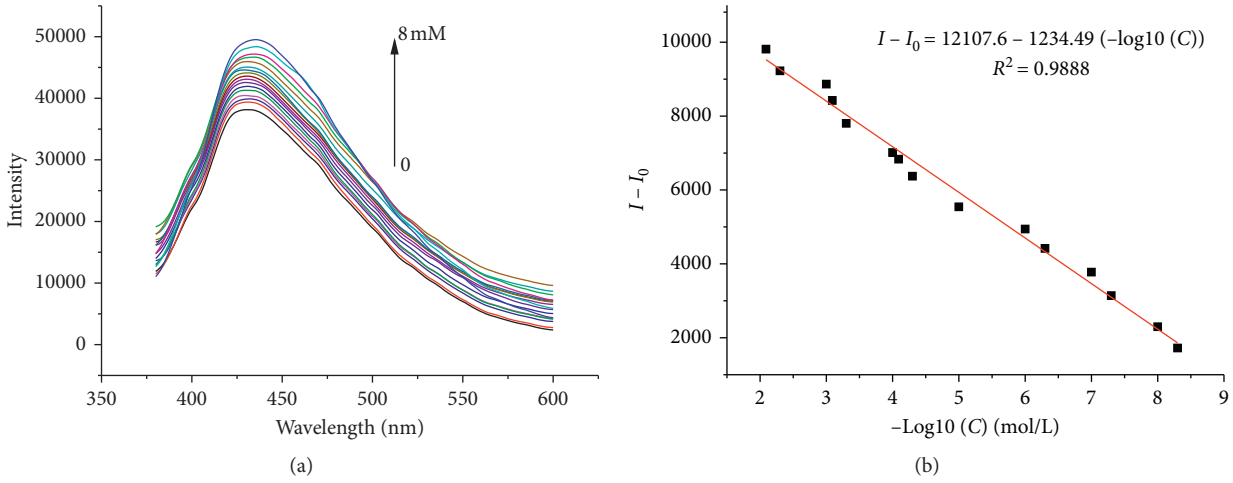


Figure 8: (a) GSH from bottom to top: 0 nM, 1 nM, 5 nM, 10 nM, 50 nM, 100 nM, 500 nM, 1 $\mu$M, 10 $\mu$M, 100 $\mu$M, 500 $\mu$M, 800 $\mu$M, 1 mM, 5 mM, and 8 mM. (b) The linear calibration ranges of the fluorescence recovery to GSH concentrations.

## 4. Conclusions

In this research, L-histidine-protected Ag NCs were prepared by the simple synthesis process. The Ag NCs were the monodisperse spheres with an average particle size of 4.15 nm. The Ag NCs could be utilized for selective detection of $Cu^{2+}$ and $Fe^{3+}$ by simply adjusting the pH value of the Ag NCs solution without using the masking agent. And a fluorescent sensing system was further built for the detection of GSH. Based on the above method, a low LOD of the $Cu^{2+}$ and GSH could be obtained.

## Data Availability

The data used to support the findings of this study are available from the corresponding author upon request.

## Conflicts of Interest

The authors declare that they have no conflicts of interest regarding the publication of the paper.

## Supplementary Materials

Table S1: the fluorescent lifetime of the Ag NCs. Figure S1: the HR-TEM image of the Ag NCs. The yellow line labels the lattice distance of the Ag. Figure S2: fluorescence spectrum of His solution (red), solution mixed with His and AgNO3 (blue), and Ag NCs solution (black) excited at 365 nm. Figure S3: fluorescence response of the Ag NCs upon addition of different concentrations of Cu2+ from top to bottom: 0 mM, 1 mM, 2 mM, 4 mM, 6 mM, and 8 mM. Figure S4: time-resolved fluorescence spectrum of the Ag NCs upon addition of different concentrations of Cu2+: 0,1 mM and 1 nM. Figure S5: TEM images of the Ag NCs in the presence of Cu2+: (a) 1 mM. (b) 1 nM. (*Supplementary Materials*)

## Acknowledgments

This work was supported by the National Key Research and Development Program of China (Grant no.

2018YFC1604204), the Key Research and Development Program of Jiangsu Province (no. BE2020756), the National First-Class Discipline Program of Food Science and Technology (Grant no. JUFSTR20180302), and the Jiangsu Province Post-Doctoral Fund (Grant no. 2019K241).

## References

[1] M. B. Stein, D. Blayney, T. Feit et al., "Acute iron poisoning in children," *Western Journal of Medicine*, vol. 125, no. 4, pp. 289–297, 1976.

[2] F. M. Henretig and A. R. Temple, "Acute iron poisoning in children," *Emergency Medicine Clinics of North America*, vol. 2, no. 1, pp. 121–132, 1984.

[3] J. L. Robotham and P. S. Lietman, "Acute iron poisoning," *American Journal of Diseases of Children*, vol. 134, no. 9, pp. 875–879, 1980.

[4] E. Tiffany-Castiglioni, S. Hong, and Y. C. Qian, "Copper handling by astrocytes: insights into neurodegenerative diseases," *International Journal of Developmental Neuroscience*, vol. 29, no. 8, pp. 811–818, 2011.

[5] O. Bandmann, K. H. Weiss, and S. G. Kaler, "Wilson's disease and other neurological copper disorders," *The Lancet Neurology*, vol. 14, no. 1, pp. 103–113, 2015.

[6] Y. H. Hung, A. I. Bush, and R. A. Cherny, "Copper in the brain and Alzheimer's disease," *JBIC Journal of Biological Inorganic Chemistry*, vol. 15, no. 1, pp. 61–76, 2010.

[7] G. E. Batley, *Trace Element Speciation Analytical Methods and Problems*, CRC Press, Boca Raton, FL, USA, 1989.

[8] Y. Su, L. Qi, and X. Mu, "A fluorescent probe for sensing ferric ions in bean sprouts based on L-histidine-stabilized gold nanoclusters," *Analytical Methods*, vol. 7, no. 2, pp. 684–689, 2015.

[9] E. Wang, A. Barati, M. B. Taherpour, and M. Shamsipur, "Determination of Hg2+ and Cu2+ ions by dual-emissive Ag/Au nanocluster/carbon dots nanohybrids: switching the selectivity by pH adjustment," *Journal of Hazardous Materials*, vol. 367, pp. 437–446, 2019.

[10] A. Zolfaghar, M. Shamsipur, and H. Abdollahi, "Hybrid of non-selective quantum dots for simultaneous determination of TNT and 4-nitrophenol using multivariate chemometrics methods," *Anal. Methods*, vol. 6, no. 16, pp. 6577–6584, 2014.

[11] A. Barati, M. Shamsipur, and H. Abdollahi, "Hemoglobin detection using carbon dots as a fluorescence probe," *Biosensors and Bioelectronics*, vol. 71, pp. 470–475, 2015.

[12] F. Molaabasi, S. Hosseinkhani, and A. A. Moosavi-Movahedi, "Hydrogen peroxide sensitive hemoglobin-capped gold nanoclusters as a fluorescence enhancing sensor for the label-free detection of glucose," *RSC Advances*, vol. 5, no. 42, pp. 33123–33135, 2015.

[13] Y. Shamsipur, J. L. Huang, and L. Jia, "A turn-on fluorescent sensor for glutathione based on bovine serum albumin-stabilized gold nanoclusters," *International Journal of Analytical Chemistry*, vol. 2018, Article ID 1979684, 2018.

[14] R. Rajamanikandan and M. Ilanchelian, "Red emitting human serum albumin templated copper nanoclusters as effective candidates for highly specific biosensing of bilirubin," *Materials Science and Engineering: C*, vol. 98, pp. 1064–1072, 2019.

[15] M. Wang, S. Wang, L. Li, and X. Su, "$\beta$-Cyclodextrin modified silver nanoclusters for highly sensitive fluorescence sensing and bioimaging of intracellular alkaline phosphatase," *Talanta*, vol. 207, pp. 120315–120322, 2020.

[16] Y. Wang, C. Deng, Y. He, and G. Song, "Glutathione-protected silver nanoclusters for sensing trace-level Hg2+ in a wide pH range," *Analytical Methods*, vol. 7, no. 4, pp. 1558–1562, 2015.

[17] N. K. Ge and C. Kryschi, "A facile UV-light mediated synthesis of l-histidine stabilized silver nanocluster for efficient photodegradation of methylene blue," *Journal of Molecular Catalysis A: Chemical*, vol. 404-405, pp. 27–35, 2015.

[18] C. Liu, Y. Ding, and Q. Li, "Photochemical synthesis of glutathione-stabilized silver nanoclusters for fluorometric determination of hydrogen peroxide," *Microchimica Acta*, vol. 184, no. 7, pp. 2497–2503, 2017.

[19] X. Lin, M. I. Setyawati, A. S. Tan et al., "Highly luminescent silver nanoclusters with tunable emissions: cyclic reduction–decomposition synthesis and antimicrobial properties," *NPG Asia Materials*, vol. 5, no. 2, pp. 39–46, 2013.

[20] T. Liu, Y. Su, and H. Song, "Microwave-assisted green synthesis of ultrasmall fluorescent water-soluble silver nanoclusters and its application in chiral recognition of amino acids," *The Analyst*, vol. 138, no. 21, pp. 6558–6564, 2013.

[21] C. Lv and J. Irudayaraj, "Fluorescent Ag clusters via a protein-directed approach as a Hg(II) ion sensor," *Analytical Chemistry*, vol. 83, no. 8, pp. 2883–2889, 2011.

[22] S. Ghosh, J. R. Bhamore, N. I. Malek, and S. K. Kailasa, "Trypsin mediated one-pot reaction for the synthesis of red fluorescent gold nanoclusters: sensing of multiple analytes (carbidopa, dopamine, Cu2+, Co2+ and Hg2+ ions)," *Spectrochimica Acta Part A: Molecular and Biomolecular Spectroscopy*, vol. 215, pp. 209–217, 2019.

[23] Z. Murthy, Y. Liu, P. Liu et al., "Non-invasive detection of gastric cancer relevantd-amino acids with luminescent DNA/silver nanoclusters," *Nanoscale*, vol. 9, no. 48, pp. 19367–19373, 2017.

[24] K. Yang and Y. C. Chen, "Using protein-encapsulated gold nanoclusters as photoluminescent sensing probes for biomolecules," *Biosensors and Bioelectronics*, vol. 61, pp. 88–94, 2014.

[25] X. Yan, L. He, C. Zhou et al., "Fluorescent detection of ascorbic acid using glutathione stabilized Au Nanoclusters," *Chemical Physics*, vol. 522, pp. 211–213, 2019.

[26] P. Qian, L. Xing, and Z. Liu, "Functionalized-tryptophan stabilized fluorescent Ag nanoclusters: synthesis and its application as Hg2+ ions sensor," *Sensors and Actuators B: Chemical*, vol. 203, pp. 252–257, 2014.

[27] J. Ma, X. Ren, X. Meng, and F. Tang, "Sensitive and selective detection of Hg2+ and Cu2+ ions by fluorescent Ag nanoclusters synthesized via a hydrothermal method," *Nanoscale*, vol. 5, no. 20, pp. 10022–10028, 2013.

[28] N. Fang, J. X. Dong, S. G. Liu et al., "Multifunctional fluorescent sensors for independent detection of multiple metal ions based on Ag nanoclusters," *Sensors and Actuators B: Chemical*, vol. 264, pp. 184–192, 2018.

[29] D. H. Li, "The biological chemistry of the transition metal "transportome" of Cupriavidus metallidurans," *Metallomics*, vol. 8, no. 5, pp. 481–507, 2016.

[30] G. Hu, G. Liang, W. Zhang et al., "Silver nanoparticles with low cytotoxicity: controlled synthesis and surface modification with histidine," *Journal of Materials Science*, vol. 53, no. 7, pp. 4768–4780, 2018.

[31] Z. Jin, Z. Xing, Y. Zu et al., "Synthesis and characterization of L-histidine capped silver nanoparticles," *Materials Science and Engineering: C*, vol. 32, no. 4, pp. 811–816, 2012.

[32] Y. Tan, D. Ding, and Y. Zhen, "Amino acid-mediated 'turn-off/turn-on' nanozyme activity of gold nanoclusters for

sensitive and selective detection of copper ions and histidine," *Biosensors and Bioelectronics*, vol. 92, pp. 140–146, 2017.

[33] I. Guo, K. Várnagy, and N. Lihi, "Coordinating properties of peptides containing histidyl residues," *Coordination Chemistry Reviews*, vol. 327-328, pp. 43–54, 2016.

[34] J. J. Grenács, D. Qiao, J. Zhao et al., "Ratiometric fluorescence detection of $Hg^{2+}$ and $Fe^{3+}$ based on BSA-protected Au/Ag nanoclusters and His-stabilized Au nanoclusters," *Methods and Applications in Fluorescence*, vol. 7, no. 4, Article ID 045001, 2019.

[35] S. C. Chen, C. Y. Lin, T. L. Cheng et al., "6-Mercaptopurine-Induced fluorescence quenching of monolayer MoS2 nanodots: applications to glutathione sensing, cellular imaging, and glutathione-stimulated drug delivery," *Advanced Functional Materials*, vol. 27, no. 41, Article ID 1702452, 2017.

[36] W.-B. Tseng, C.-H. Lee, and W.-L. Tseng, "Poly(-diallydimethylammonium chloride)-induced dispersion and exfoliation of tungsten disulfide for the sensing of glutathione and catalytic hydrogenation of p-nitrophenol," *ACS Applied Nano Materials*, vol. 1, no. 12, pp. 6808–6817, 2018.

[37] Y. Zhu, W. Li, C. Ju et al., "Selective detection of glutathione based on the recovered fluorescence of BSA-AuNCs/Cu 2+ system," *Micro & Nano Letters*, vol. 14, no. 9, pp. 952–956, 2019.

[38] S. Gong, W. Cao, A. Kumar et al., "Highly sensitive simultaneous detection of mercury and copper ions by ultrasmall fluorescent DNA-Ag nanoclusters," *New Journal of Chemistry*, vol. 38, no. 4, pp. 1546–1550, 2014.

[39] N. Jin, Y. Si, Z. Sun et al., "Rapid, selective, and ultrasensitive fluorimetric analysis of mercury and copper levels in blood using bimetallic gold-silver nanoclusters with "silver effect"-enhanced red fluorescence," *Analytical Chemistry*, vol. 86, no. 23, pp. 11714–11721, 2014.

[40] F. Chen, Q. Zhang, and J. You, "Recognition and determination of multi-metal ions based on silver nanoclusters capped by polyethyleneimine with different molecular weights," *New Journal of Chemistry*, vol. 39, no. 12, pp. 9293–9298, 2015.

[41] X. Liu, L. Wang, and N. Zhang, "Ratiometric fluorescent silver nanoclusters for the determination of mercury and copper ions," *Analytical Methods*, vol. 7, no. 19, pp. 8019–8024, 2015.

[42] Z. Shangguan, D. Lu, G. Zhang, J. Yang, C. Dong, and S. Shuang, "Glutathione capped silver nanoclusters-based fluorescent probe for highly sensitive detection of Fe3+," *Sensors and Actuators B: Chemical*, vol. 202, pp. 631–637, 2014.